6
Microstructured Reactors for Fluid–Solid Systems

6.1
Introduction

Heterogeneous systems can be subdivided into three classes based on the number of phases involved:

- fluid–solid (generally one mobile phase)
- fluid–fluid (generally two mobile phases), and
- three phase reactions (generally two mobile and one fixed phase).

The fluid–solid reactions are presented in this chapter while fluid–fluid (gas–liquid, liquid–liquid) and three phase reactions are presented in the next two chapters. Fluid–solid systems cover a major class of chemical reactions and encompass both liquid–solid and gas–solid systems. In either case, the fluid phase is a single homogeneous fluid. The solid phase acts as a catalyst and its arrangement in the main reactions zone is an important and complex task.

Conventionally, fluid–solid reactions are carried out in various types of reactors, such as packed beds, fluidized/slurry, and monolith reactors as summarized in Table 6.1 [1]. Packed bed reactors are relatively simple, easy to operate and suitable for reactions that require relatively large amounts of catalyst, as they provide a high volumetric catalyst fraction of about 60%. The characteristic feature of packed bed reactors is the pressure drop of the fluid flowing through the catalytic bed. To avoid excessive pressure drop the use of catalyst pellets of 2–6 mm is necessary. But, large porous particles lower the transformation rate through diffusion limitations in the porous network and may decrease product selectivity and yield as discussed in Chapter 2.

An important issue for packed bed reactors is temperature control. Insufficient heat removal may lead to local overheating of the catalyst pellets with the consequence of rapid deactivation. Therefore, multitubular reactors with up to 35 000 parallel tubes are used in chemical industry for the temperature control of highly exothermic reactions.

Fluidized bed reactors allow improved heat management for fast exothermic reactions thus increasing the performance of gas–solid reactors, but within narrow operating windows. Fluidized bed reactors impose special demands on the mechanical stability of the catalyst and are difficult to scale-up.

Microstructured Devices for Chemical Processing, First Edition.
Madhvanand N. Kashid, Albert Renken and Lioubov Kiwi-Minsker.

Table 6.1 Different types of fluid–solid reactors, their advantages, and limitations.

Reactors	Advantages	Limitations
Randomly packed bed reactor	Easy to operate	Flow maldistribution
	Can accommodate 60–65% (volumetric) catalyst	High pressure drop
		Risk of hot spot formation
		Thermal instabilities
Fluidized bed reactor	Good heat and mass transfer	High performance only in the limited range of flow rates
	Pressure drop independent of fluid throughput	Complex hydrodynamics
		Broad residence time distribution
		Catalyst abrasion
Monolith reactor	Low pressure drop	Catalyst deposition on reactor wall is difficult
	Higher reaction rates are achieved following better heat exchange	Performance rely on quality of flow distribution in multiple channel
	Catalyst is effectively utilized	

To overcome the drawbacks of conventional catalytic reactors, structured catalysts such as monoliths, with catalyst coated static mixers, and arranged packings as applied in distillation and absorption columns may be used [2]. Monolith catalysts are widely used in environmental catalysis where large gas stream must be processed at low pressure drop. Further examples are catalytic grids, woven fabrics, felts, and foams. Structured catalysts are characterized by high porosities, ε_{struc}, in the range of 0.7–0.9, relative to randomly packed beds with porosities of typically $\varepsilon_{bed} \approx 0.4$. In general, pressure drop in structured packings is two–four times lower than in randomly packed fixed beds.

6.2 Microstructured Reactors for Fluid–Solid Reactions

Microstructured reactors (MSR) for heterogeneous catalytic processes mostly consist of a large number of parallel flow channels. At least one dimension of these channels is smaller than 1 mm, but rarely <100 µm. This leads to an increased heat transfer in the direction of the smallest dimension. The volumetric heat transfer performance in microstructured devices is several magnitudes higher than in conventional reactors. Therefore, even highly exothermic or endothermic reactions can be operated under near isothermal conditions and thermal runaway can be avoided (see Chapter 5). In addition, mass transfer between the bulk phase

and the catalytically active surface is greatly ameliorated and the transformation rate is mostly governed by the chemical kinetics. This in turn allows high specific performance and high product yield and selectivity.

6.3 Microstructured Reactors for Catalytic Gas-Phase Reactions

An easy way to design catalytic MSR consists of introducing the catalytic active phase within the microchannels in the form of powders creating a micro packed bed. Besides randomly packed beds, the use of structured catalysts is proposed and typical examples are presented here.

6.3.1 Randomly Micro Packed Beds

The randomly micro packed bed reactors are used mainly for catalyst screening [3, 4]. The advantage of this type of catalytic reactor stems from the fact that the developed catalyst used in traditional reactors can be applied. In addition, the use of fine particles greatly increases the mass transfer between the fluid bulk and the catalyst surface.

To avoid flow maldistribution in micro packed beds the particle diameter should be less than a 10th of the tube diameter ($d_p \leq d_t/10$). The residence time distribution in packed beds can be estimated with the following empirical relation valid for gas flow (Chapter 3):

$$\frac{1}{Pe_{\mathrm{ax}}} = \frac{0.3}{Re_p Sc} + \frac{0.5}{1 + 3.8/(Re_p Sc)};$$
$$\text{for } \frac{d_t}{d_p} > 15; 0.008 < Re_p < 400; 0.28 < Sc < 2.2 \tag{6.1}$$

It follows that for $L_{\mathrm{bed}} > 50 \cdot d_p$, plug flow behavior is obtained ($Bo \geq 100$).

To avoid excessive pressure drop, a cross-flow microreactor for catalyst testing and kinetic studies is proposed (Figure 6.1) [5]. As the reactor is short, a nearly uniform axial concentration can be assumed corresponding to complete backmixing. The short packed bed reactor was microfabricated in silicon. The complex cross-flow design achieves uniform flow distribution over a 25.5 mm wide but shallow catalyst bed (400 µm long, 500 µm deep) to realize sufficiently high conversions and to allow monitoring of the reactants with conventional analysis techniques. The use of catalyst particles ($d_p = 53-71$ µm) implies that conventional synthesis procedures can be used and experimental results can be translated to catalysts in macroscopic reactors. A set of complex, shallow microfabricated channels maintains a spatially uniform pressure drop irrespective of the variations in catalyst packing and allows uniform flow distribution. Quantitative analysis of transport effects indicated that temperature and concentration gradients in the catalyst bed can be neglected making this reactor a useful experimental tool for

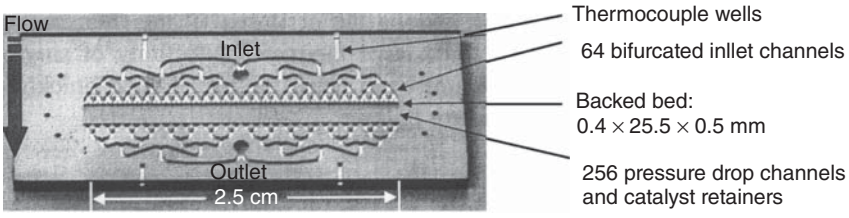

Figure 6.1 Picture of the silicon cross-flow microreactor [5]. (Reproduced from Ref. [5] with kind permission of Springer Science+Business Media.)

studying kinetics and to optimize the reaction conditions, which was proved by the experiments of CO oxidation that compared well with parameters previously determined in macroscale systems.

An integrated packed bed heat exchanger was developed for different heterogeneous catalytic reactions like methanol [6] and dimethyl ether synthesis [7]. The reactor is made of stainless steel and can be operated at pressures up to 100 bar and temperatures up to 350 °C. The device consists of rectangular slits 8.8 mm width, 0.8 or 1.5 mm height, and 60 mm length. The slit channels are filled with catalyst particles forming a micro fixed bed. The reactor channels are sandwiched between cross-flow cooling channels for effective heat transfer. Different fractions

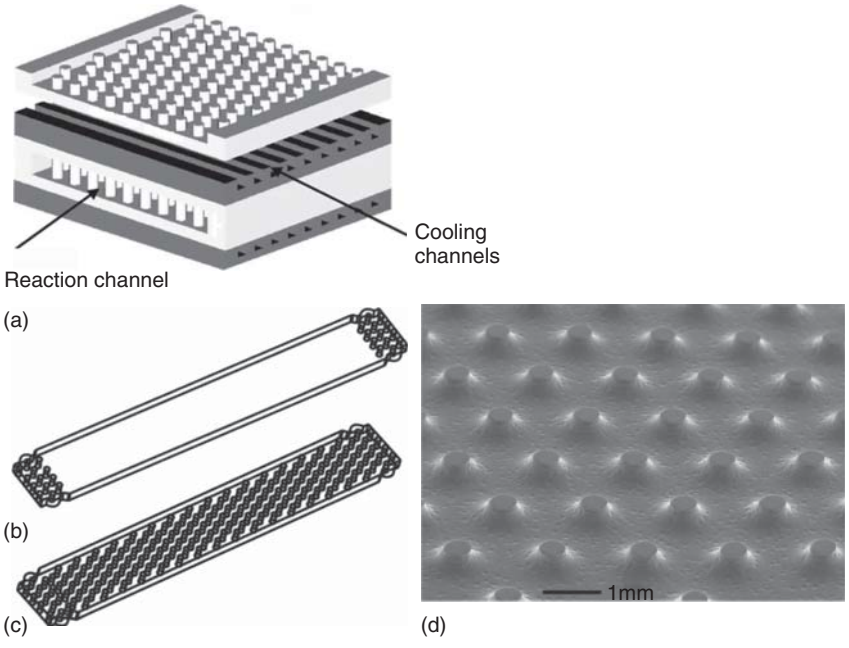

Figure 6.2 (a) Reaction slit and cooling channels arrangement, (b) pillar structure at the ends of the slit, (c) pillar structure in the whole reactor slit [7], and (d) Scanning electron microscope (SEM) picture of the pillar structure [6, 7]. (Adopted with permission from Elsevier.)

of particles between 50 μm and up to 200 μm were used to study the external mass transfer and pressure drop in the reactor. To facilitate a uniform gas distribution over the channel cross section, cylindrical pillars were introduced at the entrance and at the end, or even in the whole reactor (Figure 6.2). Near isothermal operation could be obtained with maximum temperature differences of less than 3 °C close to the entrance.

6.3.2 Structured Catalytic Micro-Beds

The drawback of randomly packed microreactors is the high pressure drop. In multitubular micro fixed beds, each channel must be packed identically or supplementary flow resistances must be introduced to avoid flow maldistribution between the channels, which leads to a broad residence time distribution in the reactor system. Initial developments led to structured catalytic micro-beds based on fibrous materials [8–10]. This concept is based on a structured catalytic bed arranged with *parallel filaments* giving identical flow characteristics to multichannel microreactors. The channels formed by filaments have an equivalent hydraulic diameter in the range of a few microns ensuring laminar flow and short diffusion times in the radial direction [10].

A microstructured string-reactor was designed for the autothermal production of hydrogen by oxidative steam reforming of methanol [10] (Figure 6.3). The main difficulty in carrying out the oxidative steam reforming is the much faster exothermic methanol oxidation compared to the endothermic reforming reaction. As a consequence, heat is generated mostly at the reactor entrance, whereas the heat consumption occurs in the middle and rear of the reactor. Metal-based catalysts with high thermal conductivity can help to integrate the exothermic combustion of methanol and the endothermic steam reforming avoiding important axial temperature profiles. The design of the microstructured string-reactor is based on catalytically active wires placed in parallel into a tube forming small channels of diameter about 100 μm. The heat generated during methanol oxidation at the reactor entrance is efficiently transferred to the reactor zone of the endothermic steam reforming. Brass metal wires (Cu/Zn = 4/1) were used as precursors for the

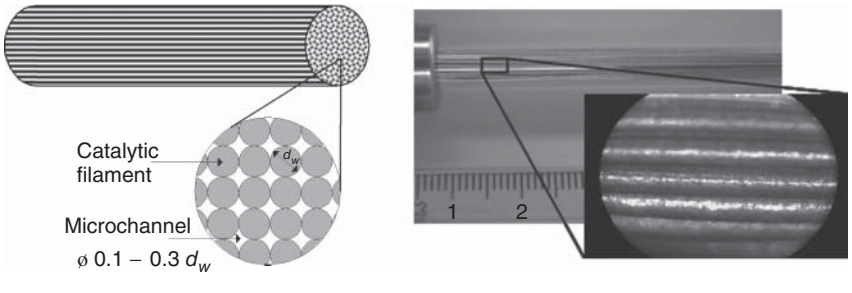

Figure 6.3 Schematic presentation and photograph of the microstructured string reactor [9]. (Adapted with permission from Elsevier.)

preparation of string-catalysts. The brass wires have high thermal conductivity (120 W m^{-1} K^{-1}) and the chemical composition is similar to the active phase of the $Cu/ZnO/Al_2O_3$ in traditional catalysts for the steam reforming of methanol. The catalyst is developed by metal/aluminum alloy formation on the outer surface of wires followed by an acid treatment leaching out aluminum. This treatment leads to an increase of the specific surface area (SSA) because of the formation of porous outer layer on the wire surface [11].

In a second example, a filamentous microstructured catalyst was used in a membrane reactor specially developed for the continuous production of propene from propane via nonoxidative dehydrogenation. The catalytic filaments with a diameter of about 7 μm consisted of a silica core covered by a γ-alumina porous layer on which an active phase of Pt/Sn is supported [8].

The catalytic filaments were introduced into the tubular reactor in the form of threads. A bundle of ~100 filaments with a diameter of ~7 μm each formed threads of diameter of about 0.5 mm. The catalytic threads were placed in parallel into the tube to form a cylindrical catalytic bed of several centimeters' length. This arrangement gives about 300 threads per cm^2 within the tube cross section with a porosity of $\varepsilon_{struc} = 0.8$. The specific surface per volume is in the order of 10^8 m^2 m^{-3} and, thus, about 50 times higher compared to washcoated tubes of the same inner diameter [8]. The performance comparison under identical experimental conditions with randomly packed beds with particles of silica and γ-alumina of different shapes and sizes showed significantly broader residence time distribution compared to the structured filamentous packing with about five times lower pressure drop for the same hydraulic diameter and comparable gas flow rates.

Reactor channels filled with *metallic or ceramic foams* as catalyst supports demonstrate several advantages compared to randomly packed beds [12]. Open cell foams consist of a network of interconnected solid stunts-building cavities

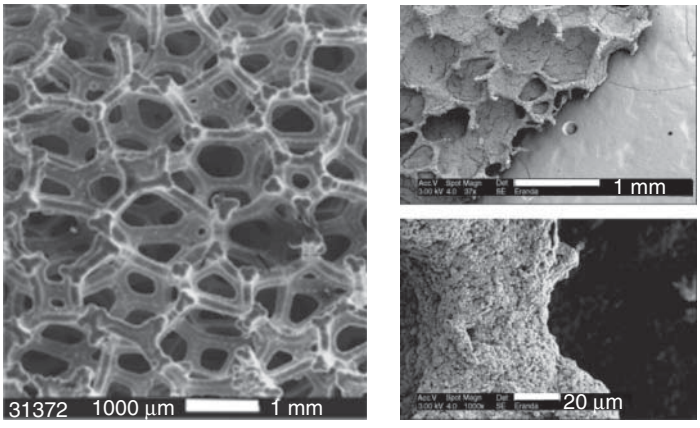

Figure 6.4 (a) Photograph of metallic foam and (b) metallic foam washcoated with catalyst [13]. (Adapted with permission from Elsevier.)

(cells). Metallic foams have porosities of up to 95% and the porosity of ceramic foams lay between 75 and 85%. Examples are shown in Figure 6.4.

Foams were proved to be highly suitable as catalytic carrier when low pressure drop is mandatory. In comparison to monoliths, they allow radial mixing of the fluid combined with enhanced heat transfer properties because of the solid continuous phase of the foam structure. Catalytic foams are successfully used for partial oxidation of hydrocarbons, catalytic combustion, and removal of soot from diesel engines [14]. The integration of foam catalysts in combination with microstructured devices was reported by Yu *et al.* [15]. The authors used metal foams as catalyst support for a microstructured methanol reformer and studied the influence of the foam material on the catalytic selectivity and activity. Moritz *et al.* [16] constructed a ceramic MSR with an inserted SiC-foam. The electric conductive material can be used as internal heating elements and allows a very rapid heating up to temperatures of 800–1000 °C. In addition, heat conductivity of metal or SiC foams avoids axial and radial temperature profiles facilitating isothermal reactor operation.

Slit-like channels can be filled with highly porous foams integrated in MSR allowing near isothermal operation for fast exo- or endothermic reactions. Compared to wall coated catalytic multichannel reactors, the foam catalyst can be easily changed in case of catalyst deactivation. An example for MSR with integrated foam is shown in Figure 6.5. The foam plates are 60 mm wide, 200 mm long, and about 1.5 mm high. They are sandwiched between plates provided with rectangular parallel cooling channels in the submillimeter range.

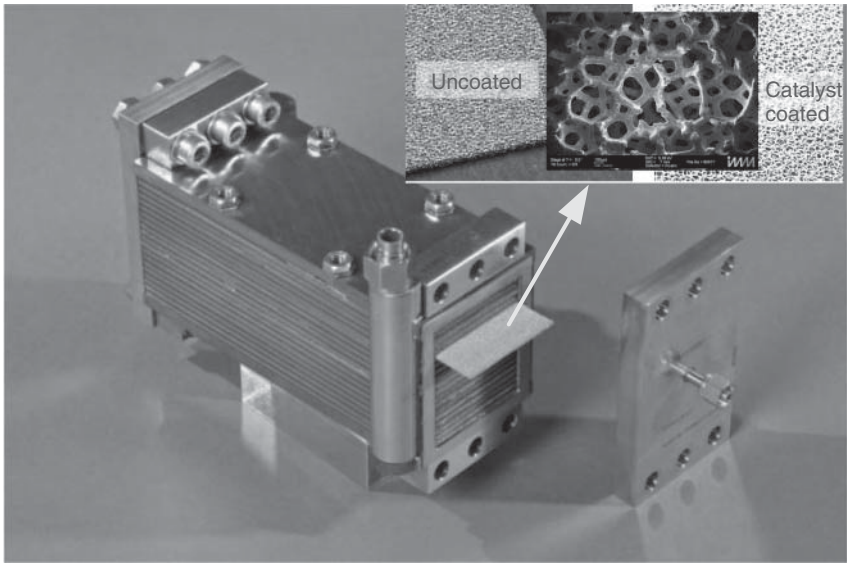

Figure 6.5 Microstructured reactor with integrated exchangeable catalytic foam plates. (Courtesy Fraunhofer ICT-IMM, Germany.)

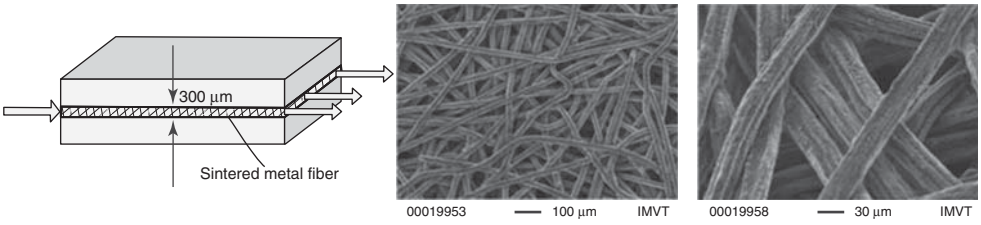

Figure 6.6 (a) Schematic presentation of a "sandwich" reactor and (b) SEM images of sintered metal fiber (SMF) catalyst. (Reproduced from Ref. [22]. Copyright © 2008, John Wiley & Sons.)

An alternative to foams are fibrous materials in the form of *tissues* or *sheets* [17–19]. Of particular interest for MSR are sintered metal fibers (SMF) sheets [18, 19]. They have an open and homogeneous structure with porosities of 70–90% and a high thermal conductivity, which ensures homogeneous temperatures in the catalytic bed. SMF consist of thin metallic fibers of 10–20 µm diameter sintered together in the form of thin (300–600 µm) sheets, thus, ensuring high external fluid–solid mass transfer performance [20]. The fibers can be covered by a homogeneous layer of zeolites [20], or oxide washcoat, which can be impregnated with an active material [21]. A SMF catalyst integrated in an MSR in the form of a sheet "sandwiched" between two metallic plates is shown in Figure 6.6 [21]. The resulting packed microchannel is 400 µm deep, 20 mm wide, and 20 mm long [21], which was used for CO oxidation under forced oscillating temperatures.

6.3.3
Catalytic Wall Microstructured Reactors

Small dimensions of the channels, a high surface-to-volume ratio together with the integrated heat exchange are the key features of the multichannel microreactors as compared to traditional reactors. The major characteristics of these reactors are discussed to quantify the potential gain in the reactor performance by structuring the fluid flow into parallel channels and by accelerating the heat supply and the heat removal. The typical configuration of a microstructured multichannel reactor with a wall catalyst is shown in Figure 6.7. The multichannel reactor is characterized by the wall thickness (e, e_{sw}) and the height (H) and width (W) of the channels.

The catalytic wall reactor with channel diameter in the range of 50–1000 µm and a length dependent on the reaction time required circumvents the shortcomings of micro packed beds. This is discussed in more detail in Section 6.5.4. However, in most of the cases, the catalytic surface area provided by the walls alone is insufficient for the chemical transformation and, therefore, the SSA has to be increased by the chemical treatment of the channel walls, or by coating them with highly porous support layers. The thickness of the layer δ_{cat} depends on catalytic activity. In general, the layer thickness is sufficiently small to avoid internal heat and mass transfer influences. Catalytic layers can be obtained by using a

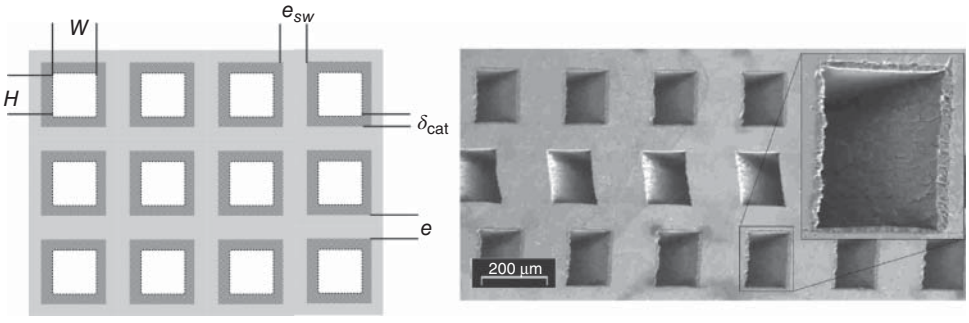

Figure 6.7 (a) Scheme of a wall coated microstructured multichannel reactor. (b) Scanning electron microscopy image of a cross section of a diffusion welded and subsequently anodically oxidized microstructured aluminum reactor. (Reproduced with permission from Ref. [23]. Copyright CHIMIA.)

Table 6.2 Different techniques used to increase surface area in catalytic wall mictrostructured reactors.

Coating layer	Technique
	Metal oxide coatings
Alumina [25–27]	Anodic oxidation of aluminum
Alumina [23]	Anodic oxidation of AlMg microstructured reactor wall
Alumina [28], silica [29], and titanium oxide [30]	Sol–gel technique
Alumina [31]	High-temperature treatment of Al containing steel (DIN 1.4767 FrCrAlloy)
γ-Alumina [32]	Wash-coating
Al_2O_3, ZnO, and CeO_2 [33]	Electrophoretic deposition
Zeolite [34, 35]	Zeolite-coated microchannel reactors
Zeolite [36–38]	Direct formation of zeolite crystals on metallic structure
Alumina [39]	Chemical vapor deposition (CVD)
Au/TiO_2 porous catalyst [40]	Flame spray
	Carbon based coatings
Carbon coating [41]	Carbonization of polymers
Carbon nanofibers [42]	Thermal chemical vapor deposition

variety of techniques such as sol–gel, electrophoretic, and chemical vapor deposition (CVD) or physical vapor deposition (PVD) [24]. Different methods of the deposition of film on the solid surface are presented in Table 6.2 as examples.

6.4 Hydrodynamics in Fluid–Solid Microstructured Reactors

The pressure drop during the passage of a fluid through a reactor is an important parameter related to the optimization of the energy consumption. Pressure

drop is considered with the assumption of noncompressible fluids and standard continuum mechanics. For example, gas properties at temperatures up to ~600 K, at a minimum pressure of 0.1 MPa with fluid velocities <10 m s^{-1} for a channel with hydraulic diameters less than 1 mm, the fluid flow is laminar and compressibility effects can be neglected [43]. The validity of the continuum assumption has been described in the previous chapter in terms of Knudsen coefficient.

The pressure drop in the fixed bed reactors packed with edged particles can be estimated using the Ergun equation [44]:

$$\frac{\Delta p}{L_{\text{bed}}} = 150\frac{(1-\varepsilon_{\text{bed}})^2}{\varepsilon_{\text{bed}}^3}\frac{\mu \cdot u}{\overline{d}_p^2} + 1.75\frac{(1-\varepsilon_{\text{bed}})}{\varepsilon_{\text{bed}}^3}\frac{\rho u^2}{\overline{d}_p} \tag{6.2}$$

where ε_{bed} is the porosity of the bed and u the superficial flow velocity, ρ and μ are fluid properties. The first term in Equation 6.2 is referred to as *viscous term* while the second term as *inertial term*. The particles are characterized by the Sauter diameter, which can be calculated from the measured particle size distribution:

$$\overline{d}_p = \left(\sum_{i=1}^{n}\frac{V_i}{V}\frac{1}{d_{p,i}}\right)^{-1} \tag{6.3}$$

with V_i/V the volume fraction of the ith particle size.

Depending on the shape and porosity of the particles, the constants in Equation 6.2 may change and must be determined experimentally.

For fixed beds consisting of mono-sized spherical particles, a modified Ergun equation is proposed [44] (and demonstrated in Example 6.1):

$$\frac{\Delta p}{L_{\text{bed}}} = 160\frac{(1-\varepsilon_{\text{bed}})^2}{\varepsilon_{\text{bed}}^3}\frac{\mu \cdot u}{d_p^2} + 3.1\frac{(1-\varepsilon_{\text{bed}})}{\varepsilon_{\text{bed}}^3}\frac{\rho u^2}{d_p}\left(\frac{\mu\left(1-\varepsilon_{\text{bed}}\right)}{\rho u d_p}\right)^{0.1} \tag{6.4}$$

Example 6.1: Pressure drop in packed bed microstructured reactors

Estimate the pressure drop of a packed bed reactor with the length of 0.1 m, porosity of 0.36, 0.4, 0.45, mean particle diameter of 100 μm, and superficial gas velocity of $u = 0.1$ m s^{-1}.

Fluid properties: density $\rho = 1$ kg m^{-3}, dynamic viscosity $\mu = 18{\cdot}10^{-6}$ Pa s.

Solution:

The pressure drop is investigated using Equation 6.2 for $\varepsilon = 0.4$ as

$$\begin{aligned}\frac{\Delta p}{L_{\text{bed}}} &= 150\frac{(1-\varepsilon_{\text{bed}})^2}{\varepsilon_{\text{bed}}^3}\frac{\mu \cdot u}{\overline{d}_p^2} + 1.75\frac{(1-\varepsilon_{\text{bed}})}{\varepsilon_{\text{bed}}^3}\frac{\rho u^2}{\overline{d}_p}\\ &= 150\frac{(1-0.4)^2}{0.4^3}\frac{18\cdot 10^{-6}\times 0.1}{(100\cdot 10^{-6})^2} + 1.75\frac{(1-0.4)}{0.4^3}\frac{1\times(0.1\cdot 10^{-3})^2}{100\cdot 10^{-6}}\\ &= 1.535\,10^5\ \text{Pa}\\ \Rightarrow\ \Delta p &= 1.535\,10^5 \times L_{\text{bed}}\\ &= 1.535\,10^4\ \text{Pa} = 153.5\ \text{hPa}\end{aligned}$$

In Figure 6.8 the strong influence of the bed porosity on the pressure drop is illustrated.

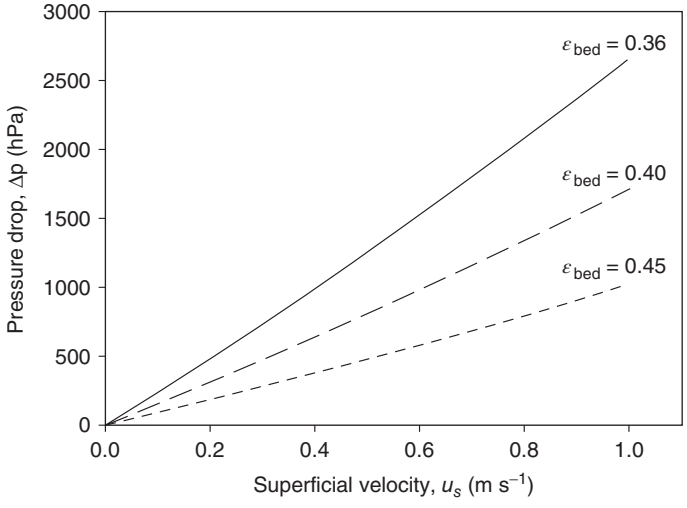

Figure 6.8 Influence of the bed porosity on pressure drop in microstructured packed bed reactors (for conditions see Example 6.1).

The pressure drop *in ceramic and metallic foams* can be estimated using the basic form of the Ergun equation [45]. Recently, Dietrich [46] evaluated the pressure drop measurements of nearly 100 different foams reported by about 25 authors. Dietrich could describe the experiments with an error of ±40% in a broad range of Re ($10^{-1} < Re < 10^5$) with the following correlation:

$$\frac{\Delta p}{L_{\text{foam}}} = 110 \cdot \frac{\mu}{\varepsilon_{\text{foam}} \cdot d_h^2} u + 1.45 \cdot \frac{\rho}{\varepsilon_{\text{foam}}^2 \cdot d_h} u^2 \tag{6.5}$$

The hydraulic diameter d_h in Equation 6.5 is defined with the porosity, $\varepsilon_{\text{foam}}$, and the SSA per foam volume a_{foam} as defined in Equations 6.6 and 6.7.

$$a_{\text{foam}} = \frac{\text{total surface area of the foam}}{\text{foam volume}} = \frac{A_{\text{foam}}}{V_{\text{foam}}} \tag{6.6}$$

$$d_h = 4 \cdot \frac{\varepsilon_{\text{foam}}}{a_{\text{foam}}} \tag{6.7}$$

The SSA a_{foam} can be obtained experimentally by computer tomography or magnetic resonance imaging measurements. The surface area can also be estimated based on the inner pore diameter d_p and the thickness of the struts d_s as illustrated in Figure 6.9 [45].

$$a_{\text{foam}} = 2.87 \left(\frac{1}{d_p + d_s} \right) (1 - \varepsilon_{\text{foam}})^{0.25} \tag{6.8}$$

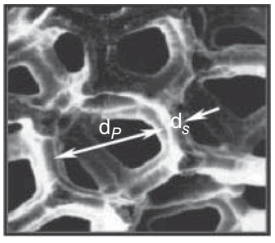

Figure 6.9 Details of a foam structure. (Adapted with permission from Ref. [14] Copyright (2003) American Chemical Society.)

The pressure drop through open channels with laminar flow is given by the Hagen-Poiseuille equation presented in Chapter 4. The geometric factor depends on the H/W ratio of rectangular channels.

$$\Delta p = 32\zeta \frac{\mu u}{d_t^2} L_t \tag{6.9}$$

$$\zeta = 0.8735 + 0.6265 \exp\left(-3.636 \frac{H}{W}\right) \tag{6.10}$$

The comparion of pressure drop in three different types of microstructured reactors, foam reactor, square channels and packed bed, is shown in Example 6.2.

Example 6.2: Comparison of pressure drop in microstructured packed bed reactor, microchannel reactor and foam reactor

Estimate the pressure drop in a metallic foam with a porosity of $\varepsilon_{\text{foam}} = 0.9$ and a SSA of $a_{\text{foam}} = 5000\,\text{m}^2\,\text{m}^{-3}$ and compare the result with pressure drop in a microstructered reactor with square channels and a micro packed bed reactor with a porosity of $\varepsilon_{\text{bed}} = 0.4$. The three devices should have the same surface area referred to the volume occupied by the fluid, commonly called void volume $V_{v,\,\text{foam}}$.

Solution:

As the three reactors have different porosities, the surface area will be referred to the void volume occupied by the fluid to get comparable conditions. For the foam, the volume of the fluid $V_{v,\,\text{foam}}$ corresponds to 90% of the foam volume. The SSA referred to $V_{v,\,\text{foam}}$ is $a_{v,\,\text{foam}} = \frac{A_{\text{foam}}}{V_{v,\,\text{foam}}} = \frac{A_{\text{foam}}}{V_{\text{foam}}} \frac{1}{\varepsilon_{\text{foam}}} = \frac{a_{\text{foam}}}{\varepsilon_{\text{foam}}}$; $\frac{A_{\text{foam}}}{V_{v,\,\text{foam}}} = a_v = 5556\,\text{m}^2\text{m}^{-3}$

The same SSA a_v is imposed for the two other microstructured reactors. The volume of the microchannel corresponds to the volume occupied by the fluid. Therefore, $a_v = a = 4/d_h$, with d_h as the hydraulic diameter of the channel. In consequence, channels with a hydraulic diameter of $d_h = 720\,\mu\text{m}$ have the required SSA of $5556\,\text{m}^2\,\text{m}^{-3}$.

The surface area in packed beds is related to the particle diameter and the SSA of a spherical particle is given by $a_P = 6/d_P$. This corresponds also to the surface area referred to the solid phase in the packed bed. The following

relationships are obtained: $a_{\text{bed}} = \frac{N \cdot A_P}{V_{\text{bed}}} = \frac{N \cdot A_P}{N \cdot V_P}(1 - \varepsilon_{\text{bed}}) = a_P(1 - \varepsilon_{\text{bed}})$; $a_v = \frac{a_{\text{bed}}}{\varepsilon_{\text{bed}}} = a_P \frac{1-\varepsilon_{\text{bed}}}{\varepsilon_{\text{bed}}}$. As a result, we find that a particle diameter of $d_p = 1.62$ mm is necessary to get a SSA of $a_v = 5556\ \text{m}^2\ \text{m}^{-3}$.

Now we can estimate the pressure drop in all devices with the presented relations Equations 6.5 and 6.7 for the foam; Equations 6.9 and 6.10 for the microchannel reactor and Equation 6.4 for the packed bed with spherical particles. For the microchannel reactor we suppose that 60% of the cross section of the reactor is occupied by the channel walls and catalytic layer (see Figure 6.7). Therefore, the channel volume available for the fluid corresponds to the void volume in the packed bed i.e. $\varepsilon_{\text{bed}} = 0.4 = \varepsilon_{\text{struc}}$. For a given superficial fluid velocity u, the velocity in the void volume is given by $u_v = u/\varepsilon_{\text{bed}}$. From Figure 6.10 it becomes evident that the pressure drop in packed bed reactors are several times higher than in foam reactors. The difference can be explained by the high porosity in the foam ($\varepsilon_{\text{foam}} = 0.9$) compared to the packed bed ($\varepsilon_{\text{bed}} = 0.4$). The lowest pressure and, therefore, the lowest energy dissipation is found for the multichannel microreactor.

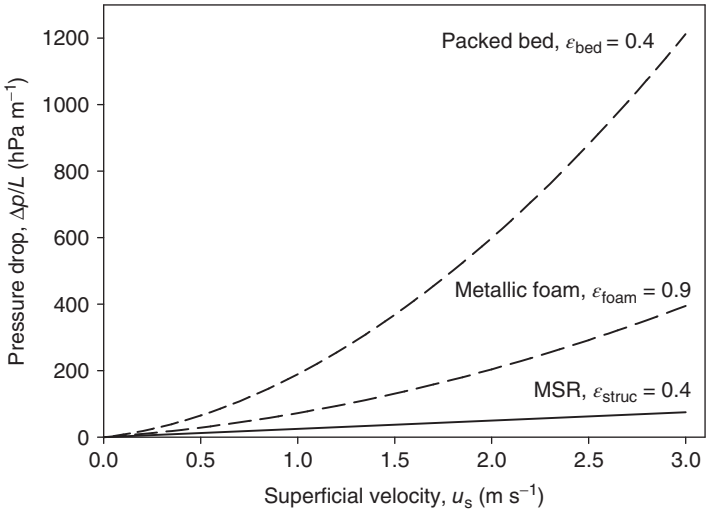

Figure 6.10 Comparison of microstructured reactors (MSR) with identical specific surface area. Physical properties of air 20 °C (see Example 6.2 for details).

6.5 Mass Transfer in Catalytic Microstructured Reactors

As described in Chapter 2, prior to catalytic heterogeneous reaction, which takes place on the surface of a solid catalyst, the reactant molecules have to first reach

the catalyst surface and, therefore, the rate of mass transfer is an important operational parameter. Two types of mass transfer need to be considered in fluid–solid reactions (Chapter 2): external and internal mass transfer. Mass transfer influences should be avoided, as they diminish the performance of the reactor and strongly affect product yield and selectivity.

In the present chapter we focus our discussion on external mass transfer in MSR. Thus, we assume that the reactions occur on the outer surface of the catalyst particle or of the wall catalytic layer. The observable effective reaction rate is determined by the ratio of the characteristic mass transfer time, t_m, and the characteristic reaction time, t_r, commonly known as *second Damköhler number DaII* (see Section 2.6.1).

$$DaII = \frac{t_m}{t_r} = \frac{k_r c_{1,b}^{n-1}}{k_m a} \tag{6.11}$$

The characteristic mass transfer time is given by the mass transfer coefficient in the fluid, k_m, and the specific outer surface area of the catalyst, a.

$$t_m = \frac{1}{k_m a} = \frac{V}{k_m A} \tag{6.12}$$

where A is the catalytically active surface of the catalyst and V is the reaction volume. To eliminate mass transfer influence in practice, the characteristic transfer time should be roughly 1 order of magnitude smaller than the characteristic reaction time.

Low values of $DaII$ ($t_m \ll t_r$) correspond to a situation where the effect of mass transfer can be neglected and the observed reaction rate is close to the intrinsic rate:

$$-R_{1,\text{eff}} \cong k_r c_{1,b}^n \tag{6.13}$$

At high values of $DaII$ ($t_m \gg t_r$) the rate of the transformation is completely controlled by mass transfer from the bulk of the fluid phase to the catalyst surface, with the surface concentration being nearly zero ($c_{1,s} \cong 0$):

$$-R_{1,\text{eff}} \cong k_m a \cdot c_{1,b} \tag{6.14}$$

6.5.1 Randomly Packed Bed Catalytic Microstructured Reactors

To avoid internal mass transfer, the diameter of porous catalyst particle must be sufficiently small. Criteria for negligible internal and external mass transfer influences are presented in Table 2.2.

In addition, the use of fine particles greatly increases the rate of external mass transfer between the fluid bulk and the catalyst surface in randomly micro packed beds. The external mass transfer coefficient can be estimated by using Equation 6.15 [47]:

$$\begin{aligned} Sh_p &= 0.91 \cdot Re_p^{0.49} \cdot Sc^{1/3}; 0.01 < Re_p \leq 50 \\ Sh_p &= 0.61 \cdot Re_p^{0.59} \cdot Sc^{1/3}; 50 < Re_p < 1000 \end{aligned} \tag{6.15}$$

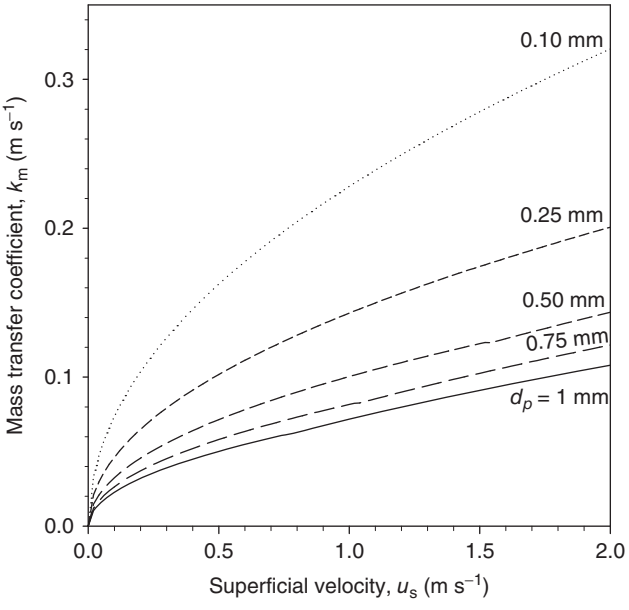

Figure 6.11 Mass transfer in micro packed bed reactors as function of superficial velocity with the particle size as parameter. ($Sc = 1$; $\varepsilon_{bed} = 0.5$; $\mu = 18 \cdot 10^{-6}$ Pa s; $\rho = 1.2$ kg m^{-3}).

where Re_p is the particle Reynolds number $Re_p = (u\, d_p)/\nu$; Sc is the Schmidt number $Sc = \nu/D_m$; and Sh_p is the particle Sherwood number $Sh_p = (d_p\, k_m)/D_m$.

The external mass transfer coefficient, k_m, increases with decreasing particle diameter and increasing linear fluid velocity, as illustrated in Figure 6.11.

6.5.2 Catalytic Foam Microstructured Reactors

The mass transfer coefficient in solid open foams can be estimated based on relations similar to those presented for packed beds.

$$Sh_{foam} = A \cdot Re_{foam}^{B}\, Sc^{1/3} \tag{6.16}$$

Incera Garrido and Kraushaar-Czarnetzki [48] introduced a geometric factor F_g to Equation 6.16 in order to get a general mass transfer correlation applicable for foams with different cell geometry. On the basis of experimental studies, they proposed the following relationship for foams with porosities in the range of $0.75 \le \varepsilon_{foam} \le 0.85$ and cell diameters of $0.87 \le d_c \le 3.13$ mm, with $d_c = d_p + d_s$ (see Figure 6.9):

$$Sh_{foam} = 1.0 \cdot Re_{foam}^{0.47} \cdot Sc^{1/3} \cdot F_g \tag{6.17}$$

with $Re_{foam} = \frac{u \cdot d_c}{\nu}$, $Sc = \frac{\nu}{D_m}$, and $F_g = \left(\frac{d_c}{0.001}\right)^{0.58} \cdot \varepsilon_{foam}^{0.44}$

For anisotropic foams a further variation of Equation 6.17 was proposed [49]. For this relationship the form-factor F_g was modified by introducing three axis describing the pore geometry. But the measurement of all pore dimensions is quite demanding and, therefore, is not presented.

6.5.3 Catalytic Wall Microstructured Reactors

To ensure an internal effectiveness factor of $\eta_p \geq 0.95$ in an isothermal catalyst layer (Figure 6.7), the following criterion must be fulfilled (see Chapter 2) [50]:

$$\delta_{\text{cat,max}} \leq b\sqrt{\frac{D_{\text{eff}} c_s}{r_{\text{eff}}}} \tag{6.18}$$

where D_{eff} and r_{eff} are the effective molecular diffusion coefficient and the observed reaction rate, respectively. The coefficient b depends on the formal reaction order and has a value of 0.8, 0.3, and 0.18 for zero, first, and second order reactions, respectively.

In the case of strong exothermic and endothermic reactions, the reactions may give rise to a temperature profile within the catalytic layer, which is dependent on reaction enthalpy (ΔH_r), activation energy (E), and the thermal conductivity of the porous catalytic material (λ_{eff}). For quasi-isothermal behavior, the observed rate, r_{eff}, should not differ from the rate that would be observed at constant temperature by >5%, and thus the resulting criterion for effective isothermal catalytic wall behavior is given by:

$$\delta_{\text{cat,max}} \leq 0.3\sqrt{\frac{R}{E}\frac{\lambda_{\text{eff}} T_s^2}{|\Delta H_r| r_{\text{eff}}}} \tag{6.19}$$

where T_s corresponds to the temperature of the catalyst surface and R is the gas constant.

In general, the thickness of the catalytic layer is kept sufficiently small to avoid the influence of internal mass transfer on the kinetics. In this way, only the transfer of the reactants from the bulk of the fluid to the catalytic wall and the reaction rate per unit of the outer surface of the catalytic layer must be considered.

Because of the small diameters of microchannels, laminar flow can be assumed. The radial velocity profile in a single channel develops from the entrance to the position where a complete Poiseuille profile is established. The length of the hydrodynamic entrance zone (L_e) in a circular tube depends on the Re ($= \rho u d_t/\mu$) and can be estimated from the following empirical relation [51, 52]:

$$L_e \leq 0.06 \cdot Re \cdot d_t \tag{6.20}$$

Within the entrance zone, the concentration profile can be developed and the mass transfer coefficient diminishes reaching a constant value. The

Table 6.3 Mass transfer characteristics for different channel geometries [53].

Geometry	Sh_∞
Circular	3.66
Ellipse ($W/H = 2$)	3.74
Parallel plates	7.54
Square	2.98
Equilateral triangle	2.47
Sinusoidal	2.47
Hexagonal	3.66

dependency can be described with (Equation 6.21) in terms of Sherwood numbers, $Sh = k_m d_h / D_m$ [53, 54]:

$$Sh = Sh_\infty \left(1 + 0.095 \frac{d_h}{L} Re \cdot Sc \right)^{0.45} \tag{6.21}$$

where, Sc is Schmidt number ($Sc = \mu / \rho D_m$). Sh_∞ is the asymptotic Sh for constant concentration at the wall, which is identical to the asymptotic Nusselt number Nu, characterizing the heat transfer in laminar flow at constant wall temperature. The asymptotic Sh depends on the geometry of the channel as summarized in Table 6.3.

For rectangular channels, Sh_∞ depends on the ratio between channel height, H, and width, W (Figure 6.7), and can be estimated with the following correlation:

$$Sh_\infty = 2.8932 + 4.6482 \exp\left(-4.4754 \frac{H}{W} \right) \tag{6.22}$$

It follows for a circular-shaped reactor:

$$Sh_\infty = 3.66; \quad \text{for } L \geq 0.05 Re \cdot Sc \cdot d_h \quad \text{(constant wall concentration)} \tag{6.23}$$

The entrance length estimation is demonstrated in Example 6.3.

Thus, the mass transfer coefficient can be calculated as

$$k_m = \frac{Sh_\infty D_m}{d_h} \tag{6.24}$$

Example 6.3: Length of entrance zone to achieve asymptotic *Sh*-number.

Estimate the length of the entrance zone to achieve asymptotic Sh for constant concentration at the wall for rectangular (H/W = 0.5) and square channels, assuming identical operating conditions and Sh is 5% higher than Sh_∞ The gas flows with a velocity of 0.1 m s^{-1} and the diffusion coefficient is 10^{-5} m^2 s^{-1}.

Data: $\nu = 1$ m^2 s^{-1}, $d_h = 0.4$ mm.

Solution:

As the Sh is assumed to be 5% higher than Sh_∞, $Sh = 1.05Sh_\infty$. The length is investigated from Equation 6.21. Let us first solve for product $Re{\cdot}Sc$ as required

$$Re \cdot Sc = \frac{ud_h}{\nu}\frac{\nu}{D_m} = \frac{ud_h}{D_m} = \frac{0.1 \times 0.4 \cdot 10^{-3}}{1 \cdot 10^{-5}} = 4$$

and the length, say for rectangular channel with height/width ratio = 0.5, is

$$L = \frac{0.095 \cdot d_h \cdot Re \cdot Sc}{\left(\frac{Sh}{Sh_\infty}\right)^{\frac{1}{0.45}} - 1} = \frac{0.095 \cdot 0.4 \cdot 10^{-3} \cdot 4}{\left(\frac{1.05 \times 3.39}{3.39}\right)^{\frac{1}{0.45}} - 1} = 0.32 \cdot 10^{-3}\ \text{m}$$

as the ratio of Sh/Sh_∞ is constant for all channels, that is, 1.05. The length of the entrance zone to achieve asymptotic Sh is identical for all channels for identical operating conditions.

The specific performance of the MSR under mass transfer limitations depends on the mass transfer coefficient and the SSA of the channel (a):

$$a = \frac{4}{d_h} \tag{6.25}$$

with $d_h = \frac{4 \cdot A_{cs}}{l_{circ}}$ hydraulic diameter

The product $(k_m{\cdot}a)$ is called *volumetric mass transfer coefficient* (demonstrated in Example 6.4), which determines the maximal reactor performance for very fast catalytic reactions. Its value increases with $1/d_h^2$.

Example 6.4: Volumetric mass transfer coefficient for different microchannel geometries

Estimate and plot the volumetric mass transfer coefficient ($k_G a$) for different microchannel geometries such as slit, rectangle ($H/W = 0.25$), circular, and square for different hydraulic diameter ranging from 50 to 1000 µm neglecting the influence of entrance zone. The diffusion coefficient of gas (D_m) is $10^{-5}\ \text{m}^2\ \text{s}^{-1}$.

Solution:

The volumetric mass transfer coefficient for different hydraulic diameters can be investigated assuming asymptotic values of Sherwood number (Sh_∞) using Equation 6.24, the specific interfacial area using Equation 6.25. If the entrance zone in the tube is neglected, the mass transfer constant is given by

Sh_∞. Sh_∞ can be estimated with Equation 6.22 and d_t is replaced by d_h

$$k_m = \frac{Sh_\infty D_m}{d_h}$$

$$a = \frac{4}{d_h} \quad \text{for all channels.}$$

The calculated values are plotted in Figure 6.12.

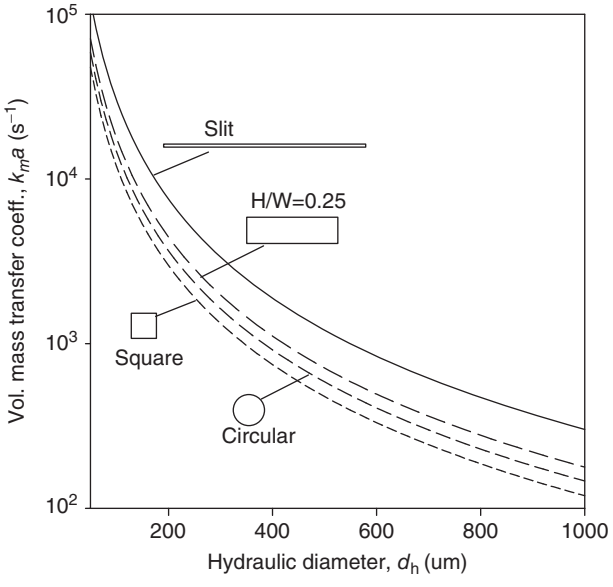

Figure 6.12 Volumetric mass transfer coefficient as function of the hydraulic diameter in microchannels ($D_m = 10^{-5}$ m^2 s^{-1}).

If the mass transfer is accompanied by a chemical reaction at the catalyst surface on the reactor wall, the mass transfer depends on the reaction kinetics [55]. For a zero-order reaction, the rate is independent of the concentration and the mass flow from the bulk to the wall is constant, whereas the reactant concentration at the catalytic wall varies along the reactor length. For this situation the asymptotic *Sh* in circular tube reactors becomes $Sh'_\infty = 4.36$ [55]. The same value is obtained when reaction rates are low compared to the rate of mass transfer. If the reaction rate is high (very fast reactions), the concentration at the reactor wall can be approximated to zero within the whole reactor and the asymptotic value for *Sh* is $Sh_\infty = 3.66$. As a consequence, the *Sh* in the reacting system depends on the ratio of the reaction rate to the rate of mass transfer characterized by the second Damköhler number defined in Equation 6.11.

Villermaux [55] proposed a simple relation to estimate the asymptotic *Sh* for mass transfer with chemical reaction (Sh''_∞) as function of *DaII*

$$\frac{1}{Sh''_{\infty}} = \frac{1}{Sh'_{\infty}} + \frac{DaII}{DaII + 1.979}\left(\frac{1}{Sh_{\infty}} - \frac{1}{Sh'_{\infty}}\right) \tag{6.26}$$

Thus, the mass transfer coefficient in multitubular MSR depends besides the molecular diffusion coefficient, on the channel diameter d_t and the second Damköhler number, *DaII* (refer Example 6.5):

$$k_G = \frac{Sh''_{\infty} D_m}{d_t} \tag{6.27}$$

Example 6.5: asymptotic *Sh* and mass transfer coefficient (with chemical reaction)

Estimate the asymptotic *Sh* for mass transfer with chemical reaction for a circular cross section microchannel with the diameter of 500 µm for *DaII* equal to 0.1, 1, and 100. Also, estimate the mass transfer coefficient for a gas-phase system with molecular diffusivity (D_m) of 10^{-5} m^2 s^{-1}. For circular tube $Sh_{\infty} = 3.66$ and $Sh'_{\infty} = 4.36$.

Solution:

The asymptotic *Sh* for mass transfer with chemical reaction is estimated using Equation 6.26.

For $DaII = 0.1$: asymptotic *Sh* is

$$\begin{aligned}\frac{1}{Sh''_{\infty}} &= \frac{1}{Sh'_{\infty}} + \frac{DaII}{DaII + 1.979}\left(\frac{1}{Sh_{\infty}} - \frac{1}{Sh'_{\infty}}\right)\\ &= \frac{1}{4.36} + \frac{0.1}{0.1 + 1.979}\left(\frac{1}{3.66} - \frac{1}{4.36}\right) = 0.23\\ &\Rightarrow Sh''_{\infty} = 4.32\end{aligned}$$

and the mass transfer coefficient can be calculated using Equation 6.27 as

$$\begin{aligned}k_G &= \frac{Sh''_{\infty} D_m}{d_t}\\ &= \frac{4.32 \times 1 \cdot 10^{-5}}{500 \cdot 10^{-6}} = 8.64 \cdot 10^{-2}\,\mathrm{m \cdot s^{-1}}\end{aligned}$$

Similarly,

For $DaII = 1$: $Sh''_{\infty} = 4.09$, $k_G = 8.19 \cdot 10^{-2}$ m · s^{-1}

For $DaII = 100$: $Sh''_{\infty} = 3.67$, $k_G = 7.34 \cdot 10^{-2}$ m · s^{-1}

The above example indicates that with increase in *DaII*, Sh''_{∞} decreases and attends a value close to the case of pure mass transfer. An identical behavior can be observed for mass transfer coefficient. On the other hand, the example of mass transfer with very high transformation rate in packed bed and microchannel reactor is demonstrated in Example 6.6.

In addition to appropriate mass transfer rates, sufficiently rapid heat transfer is essential to control the behavior of chemical reactors. For example, if the local

rate of heat removal does not match the rate of heat produced by the chemical reaction, hot spots will be formed. As the reaction rate depends exponentially on temperature, reactor performance, that is, product yield and selectivity, is strongly influenced by nonisothermicity. In the case of exothermic reactions, a steep local temperature rise can lead to reactor runaway. The stability criteria mentioned in Chapter 5 can be applied to investigate the reactor stability.

Example 6.6: Performance comparison of packed bed microreactor and microchannel reactor

A toxic compound in air has to be eliminated by catalytic oxidation. The concentration of the toxic must be reduced from initially 1% to <1 ppm. At 100 °C the transformation rate is very high and in consequence limited by the external mass transfer between the bulk fluid and the catalytic surface. A small catalytic packed bed with spherical particles is used to treat a gas flow of $1.5\,m^3\,h^{-1}$.

Estimate the obtainable outlet concentration under the given conditions and the pressure drop. Design a catalytic wall multichannel reactor for the same performance. The square channel should have the same SSA as the packed bed reactor referred to as the fluid (void) fraction ($a_{struc} = a_v$).

Solution:

Packed bed reactor:

To calculate the reactor performance and the pressure drop, we need the superficial velocity and the SSA. The cross section of the reactor is $A_{cs} = 5.726\,10^{-4}\,m^2$ leading to a superficial velocity of $u = \dot{V}_0/A_{cs} \Rightarrow u = 0.7278\,m\,s^{-1}$.

The SSA referred to the particle volume is $a_P = 6/d_P \Rightarrow a_P = 3333\,m^2\,m^{-3}$. It follows for the SSA referred to the volume of the packed bed: $a_{bed} = a_P \cdot (1 - \varepsilon_{bed}) \Rightarrow a_{bed} = 2000\,m^2\,m^{-3}$ and a surface area referred to the void fraction $a_V = a_{bed}/\varepsilon_{bed} = a_P \cdot (1 - \varepsilon_{bed})/\varepsilon_{bed} \Rightarrow a_V = 5000\,m^2 m^{-3}$.

The mass transfer coefficient can be estimated with Equation 6.15. With a Reynolds number of $Re_p = \frac{u \cdot d_p}{\nu} = 56.59$, the particle Sherwood number is $Sh_p = 0.61 \cdot Re_p^{0.59} \cdot Sc^{1/3}, Sh_p = 8.73$. It follows a mass transfer coefficient of $k_m = Sh_P \cdot D_m/d_P, k_m = 4.85 \cdot 10^{-2} m\,s^{-1}$ and a volumetric mass transfer coefficient of $k_m \cdot a_{bed} = 97\,s^{-1}$.

The space time in the packed bed corresponds to $\tau_{bed} = V_{bed}/\dot{V}_0 = (4.12 \cdot 10^{-5} m^3)/(4.167 \cdot 10^{-4} m^3 s^{-1}) = 0.0989 \cong 0.1$ s. The concentration at the reactor outlet can be determined assuming plug flow behavior of the reactor:

$$c_{out} = c_0 \cdot \exp(-k_m a_{bed} \cdot \tau_{bed}) = c_0 \cdot \exp(-DaI_m)$$
$$= 10\,000\ \text{ppm} \cdot \exp(-9.7) \cong 0.6\ \text{ppm}.$$

The pressure drop in the packed bed can be estimated with the modified Ergun equation (Equation 6.4) for spherical particles.

With the values in Table 6.4 we obtain $\Delta p/L_{\text{bed}} = 9.43 \cdot 10^3\,\text{Pa m}^{-1}$. The pressure drop in the short reactor of 72 mm length is $\Delta p = 6.79 \cdot 10^2\,\text{Pa} \cong 6.8\,\text{hPa}$.

Table 6.4 Reaction conditions and physical properties.

Reactor data		Physical properties (air at 100 °C, 0.1 MPa)	
Reactor diameter, d_{bed} (mm)	27	Dynamic viscosity, μ (Pa s)	$21.6 \cdot 10^{-6}$
Reactor height, L_{bed} (mm)	72	Kinematic viscosity, ν ($\text{m}^2\,\text{s}^{-1}$)	$23.15 \cdot 10^{-6}$
Void fraction, ε (-)	0.4	Density, ρ (kg m^{-3})	0.933
Particle diameter, d_P (mm)	1.8	Diffusion coefficient, D_m ($\text{m}^2\,\text{s}^{-1}$)	10^{-5}
Volumetric inlet flow, $\dot{V}_0$ ($\text{m}^3\,\text{h}^{-1}$) (100 °C, 0.1 MPa)	1.5	Schmidt number, Sc (–)	2.315
Reaction temperature, T (°C)	100	—	—

Design of a microchannel reactor:

The diameter of the square microchannels with a SSA of $a_v = a_{\text{struc}} = 5000\,\text{m}^2\,\text{m}^{-3}$ corresponds to $d_h = 4/a \Rightarrow d_h = 800\,\mu\text{m}$. With the cross sectional area of 1, $A_{\text{cs}} = 6.4 \cdot 10^{-7}\,\text{m}^2$. To obtain the same low final concentration in the catalytic wall reactor, an identical Damköhler number is required: $DaI_m = k_m a_{\text{struc}} \cdot \tau = 9.7$. A conservative estimation of the mass transfer coefficient is based on the asymptotic Sherwood number (Equations 6.22 and 6.24). With $Sh_\infty = 2.98$ a mass transfer coefficient of $k_m = 3.73 \cdot 10^{-2}\,\text{m s}^{-1}$ and a volumetric mass transfer coefficient of $k_m a_{\text{struc}} = 186\,\text{s}^{-1}$ is obtained. In consequence, a space time of $\tau = 5.2 \cdot 10^{-2}\text{s}$ is necessary to get a Damköhler number of $DaI_m = 9.7$ and a final concentration of the toxic of 0.6 ppm. To avoid an excessive pressure drop in the microchannel reactor, the gas flow must be distributed over several parallel channels. Also, the channels must be sufficiently long to achieve plug flow behavior with Bodenstein numbers $Bo \cong 100$. The Bo can be estimated with the relations presented in Chapter 3:

$$Bo = \frac{u \cdot L}{D_{ax}};\; D_{ax} = D_m + \frac{1}{\chi}\frac{u^2 d_h^2}{D_m} \cong \frac{1}{\chi}\frac{u^2 d_h^2}{D_m},\; \text{with}\; \chi = 119\,\text{for square channels}$$

$$\text{Bo} \cong \frac{\tau \cdot D_m \cdot \chi}{d_h^2} = \frac{5.3 \cdot 10^{-2} s \cdot 10^{-5} m^2 s^{-1} \cdot 119}{(0.8 \cdot 10^{-3} m)^2} = 98.6 \qquad (6.28)$$

With the short space time predicted, the Bo-number estimated is $Bo = Bo \sim 97$. Therefore, plug flow can be assumed in the microchannel

reactor. We propose to use a reactor length of $L_t = 0.072\,\mathrm{m}$, which corresponds to the length of the packed bed reactor discussed in the first part of the example.

For the treatment of $1.5\,\mathrm{m^3\,h^{-1}}$ in the microreactor with a space time of 0.052 s we need a reactor volume of $V_R = 2.17{\cdot}10^{-5}\,\mathrm{m^3}$. Therefore, we need 471 parallel channels. An MSR consisting of 20 plates and 25 channels per plate results in 500 channels sufficient for the task of toxic elimination as described at the beginning.

The pressure drop in the channel reactor can be estimated with Equation 6.9:

$$\Delta p = 32\zeta \frac{\mu u}{d_h^2} L_t = 32 \cdot 0.89 \frac{21.6 \cdot 10^{-6} \cdot 0.072/0.053}{(0.8 \cdot 10^{-3})^2} 0.072 = 94\,\mathrm{Pa}$$

Compared to the packed bed reactor the pressure drop is roughly seven times lower.

6.5.4 Choice of Catalytic Microstructured Reactors

In the previous sections, the mass transfer and the pressure drop properties of three different microstructured devices for fast catalytic reactions have been assessed. In the present chapter, we compare their mass transfer performance while considering the energy demand in order to choose an appropriate design of microreactor for an eventual catalytic reaction.

The mass transfer in forced flow is trade-off between the attainable mass transfer time, t_m, and the energy input. The nonidentical geometries of the different devices complicate the direct comparison. Therefore, dimensionless numbers are used. The mass transfer performance is characterized by the ratio between the space time of the fluid and the characteristic mass transfer time. This ratio corresponds to the first Damköhler number for mass transfer. Whereas the porosity of a packed bed reactor is mostly in the order of $0.35 < \varepsilon_{\mathrm{bed}} < 0.45$ depending on the particles' shape, the "porosity" of a multichannel microreactor may change in a wide range depending on the wall thickness, the thickness of the catalyst layer, and, finally, the presence of the cooling channels that do not contribute to the volume available for the reacting fluid. Therefore, we prefer to define the space time with the void volume of the reactor and to refer the catalytic surface area to the void volume occupied by the fluid. As the specific surface is inversely proportional to the volume and the space time is directly proportional to the volume, the Damköhler number will be independent of the chosen reference volume.

$$DaI_m = \frac{\tau_R}{t_m} = k_m a_R \tau_R = k_m a_v \tau_v = k_m \cdot \frac{A}{\dot{V}_0}; \text{with } A \text{ as the catalytic surface area} \tag{6.29}$$

The higher the value of DaI_m is, the better the mass transfer performance of the reactor for very fast, mass transfer limited processes. As the mass transfer is a first

order process, the conversion is given by:

$$-\ln(1-X) = DaI_m; X = 1 - \exp(-DaI_m) \tag{6.30}$$

The energy input for the mass transfer process can be characterized with the Euler number, which is a measure of pressure loss to the kinetic energy of the flowing fluid.

$$Eu = \frac{\Delta p}{\rho \cdot u_v^2} \tag{6.31}$$

This leads to the following relation, which can be interpreted as a mass transfer effectiveness or trade-off index [56].

$$\eta_m = \frac{DaI_m}{Eu} = \frac{k_m a_v \cdot L_t}{u_v} \cdot \frac{\rho \cdot u_v^2}{\Delta p} \tag{6.32}$$

with u_v as the interstitial velocity, which is related to the superficial velocity by the porosity (ε) of the reactor: $u_v = u/\varepsilon$.

For three types of microstructured devices – the multichannel catalytic wall microreactor, the micro packed bed, and the catalytic metallic foam – the mass transfer effectiveness was calculated with the relations for mass transfer and pressure loss given in the previous sections. For the metallic foam, characteristic data were taken from [46] and [48]. The effectiveness is not dependent on the size or length of the device.

The results are plotted as the function of the interstitial velocity in Figure 6.13. Whereas the multichannel and the foam reactor reaches transfer effectiveness of $0.35 > \eta_m > 0.1$, the values for micro packed beds is found to be between $0.006 > \eta_m > 0.002$. The highest effectiveness can be obtained with microchannel

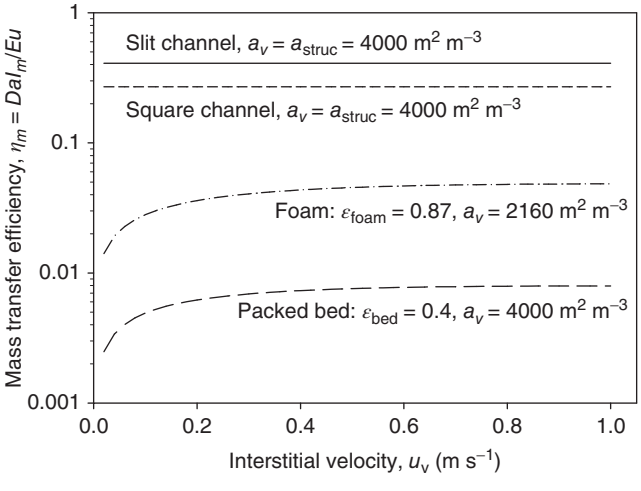

Figure 6.13 Mass transfer effectiveness for different microstructured reactors. Gas-phase, physical properties of air at 20 °C, 0.1 MPa.

reactors. The effectiveness increases with decreasing aspect ratio, H/W, of the rectangular channels. Highest values are obtained for slit-like geometries.

6.6 Case Studies

Fluid–solid MSR have been extensively used particularly for gas–solid reactions such as catalytic partial oxidations, selective hydrogenations, dehydrogenations, dehydrations, and reforming processes [57, 58]. Similarly to the other reactions carried out in MSR, the main objective was to achieve better temperature control in order to prevent selectivity loss, catalyst deactivation, hot spot formation and, thus, allowing safe processing with high throughput.

Some of the examples with a short description of reactor design, channel dimensions, methods of microreactor fabrication, and key results of their testing are described in the following.

6.6.1 Catalytic Partial Oxidations

Many partial oxidations are carried out using pure oxygen at elevated pressures. By this, space time yields can be increased. One of the initial studies was on *ammonia oxidation* in a chip-like microreactor [59] with the aim of demonstrating the feasibility of decentralized and safe production of hazardous chemicals. The reaction is highly exothermic and has several series and parallel reaction pathways allowing for selectivity studies.

The desired product of the reaction is NO, while production of N_2 represents a product loss. A single T-shaped microchannel with integrated temperature and flow sensors, etched by KOH into a silicon wafer, was covered by a SiN membrane carrying a thin-film Pt layer for heating on the outer side and a Pt catalyst layer on the inner side. A temperature as high as 800 °C was achieved in the reaction zone because of selective heating of the reactor parts; however, the experiments were limited to 650 °C, because high temperatures caused deformations and rupture of the membrane. Increasing the heating power leads to a higher NO/N_2 ratio. Higher residence time led to complete conversion and it also decreased the NO/N_2 ratio as the NO had time to re-adsorb and decompose. In ammonia-rich feed, conversion vanished because of an inhibition of NO desorption by ammonia. The small reactor had a production capacity of 10 g NO per day.

Another *silicon membrane* microreactor, composed of an aluminum bottom plate, a microstructured silicon layer carrying the channel system, and a 3 µm thick SiN membrane as a cover of the reactor, was developed [60]. Pt as an active component was put on the membrane either by wet chemistry or by PVD on a Ti adhesion layer. The reactor was manufactured by photolithography and plasma etching. The channels were introduced either by wet-etching or deep reactive ion etching. By increasing the thickness of the membrane from 1 to 1.5 and 2.6 µm,

and switching to pure silicon, the ability of the reactor membrane to dissipate heat was increased by an order of magnitude [61]. At this high temperature, a high selectivity to NO was found. The thicker membranes allowed for lower operation temperatures and thus lower NO selectivity. Introducing silicon membranes into the reactor increased the heat conductivity by 25 times, which improved the temperature uniformity. By using SiO_2 and Si_3N_4 as membrane material, stress-compensated membranes of 0.25 and 0.3 µm thicknesses could be manufactured.

A silicon-based MSR for the study of the intrinsic kinetics of the *catalytic partial oxidation of methane* was used [62]. The single microchannel was 30 mm long and a cross section of 500 × 500 µm, manufactured by photolithography, was put into a housing made of aluminum. The channel was covered by a 1.9 µm thick silicon sheet, which allowed good thermal contact between the Rh catalyst beneath it and the 5 Pt heating wires and the 12 Pt temperature sensors on top of it. Isothermal conditions of gas inlet temperature and wall side and bottom temperature generated highest Nusselt numbers and, therefore, heat transfer coefficients, which was favorable for the minimization of heat transfer of the reaction under investigation.

Microchips with catalytic wire have been applied for H_2/O_2 *oxidation reaction* in a single-channel reactor [63]. The reactor was designed as a modular and flexible tool for various high-temperature reactions. Stainless steel housing took up the silicon chips that were carrying the microchannels. The wafers were coated with silicon oxide (400 nm thickness) and silicon nitride by low-pressure chemical vapor deposition (LPCVD) alternatively. The chips were manufactured by photolithography and etching. The catalyst (for this application Pt) was introduced as a wire (150 µm thickness), which was heated resistively for igniting the reaction. The ignition of the reaction occurred at 100 °C and complete conversion was achieved at a stoichiometric ratio of the reacting species generating a thermal power of 72 W.

The same reaction was performed in a quartz glass microreactor with a diameter of 600 µm and 20 mm length [64]. The ceramic housing of the reactor and the reactor itself were stable for temperatures exceeding 1100 °C. Again, a Pt wire of 150 µm diameter was used as a catalyst and electrically heated for start-up. Residence times down to 50 µs were achieved. The fact that no homogeneous reactions, which are explosive, could be detected demonstrating the possibility of separating homogeneous and heterogeneous reactions in microreactors because of the higher surface area to the volume ratio of this reactor type.

A microstructured device consisting of a preheating unit, a mixer, a reactor, and a quenching zone was used for the exothermic *oxidative dehydrogenation of methanol to formaldehyde* [65].

The reactor was manufactured by photolithography and etching followed by the catalyst deposition and anodic bonding of the Pyrex glass cover. Silver was introduced as catalyst by sputtering. The reaction was carried out at residence times between 4 and 25 ms, temperatures between 430 and 530 °C, inlet methanol concentration of 8.5 – 8.6 vol%, and pressure slightly above atmospheric pressure. CO_2

and formic acid were found as products, the carbon monoxide formation being successfully suppressed. Increasing the residence time from 4 to 24 ms increased the conversion, but hardly affected the selectivities. Generally, in the deeper channels, higher conversion was achieved.

Further, a *chip-like* reactor for the same reaction at temperatures exceeding 600 °C was used [66] with the motivation of achieving extremely fast heating and cooling and ultrashort residence times. In an integrated heater/reactor/cooler system, the heater was composed of silicon microstructured by KOH etching and capped with an SiN membrane. The channel was 7.4 mm long and had a trapezoidal cross section 1.3 mm wide and 380 μm deep. Pt–Ta filaments were used to heat the bottom made of Pyrex. At a flow rate of 30 std cm^3 min^{-1}, which corresponds to a residence time of 4 ms, a heating power as low as 1.7 W was able to increase the exit temperature of the test gas nitrogen up to 400 °C. The heat exchanger for cooling had a counterflow design. All channels were approximately 300 μm deep and 20 mm long. The cooling fluid, nitrogen, with a rate of 500 std cm^3 min^{-1} was cooled from 500 to 54 °C in less than 1 ms by the cooler.

6.6.2 Selective (De)Hydrogenations

Hydrogenations and dehydrogenation reactions are usually highly exo-/endothermic, involve hydrogen, a very reactive compound, and, therefore, precise control of reaction conditions and safety are important issues.

Membrane MSR for the *dehydrogenation of cyclohexane* to benzene were designed [67]. This is an endothermic reaction whose equilibrium conversion is 18.9% at 200 °C. The conversion can increase beyond equilibrium up to 99% if the hydrogen is removed from the system. Therefore, a Pd-membrane with microchannels has been used to continuously remove hydrogen out of the reaction zone in order to enhance the conversion. The reactors were made of silicon using photo-etching technique, and Pt was used as a catalyst, which was sputtered onto the reaction chamber [67]. Out of two reactors, one example is shown in Figure 6.14.

A chip-like silicon-based process-engineering device consisting of a preheater, a reactor, and an integrated thermocouple mainly applying photolithographic techniques (see Figure 6.15) was fabricated and used for benzene hydrogenation [68]. The top and bottom part of the reactor was made of glass, which is attached to the silicon core by anodic bonding. The reactor was heated by an integrated Pt wire at the bottom as shown in the bottom view of Figure 6.15. Both sputtering of the silicon surface and wet impregnation of alumina precipitated by the sol–gel method were used to introduce Pt as the active component. After activation in H_2 at 500 °C, the catalyst was tested for benzene hydrogenation at temperatures between 100 and 150 °C, a flow rate of 1 cm^3 min^{-1}, and residence times from 100 to 600 ms. First order kinetics were found for the reaction.

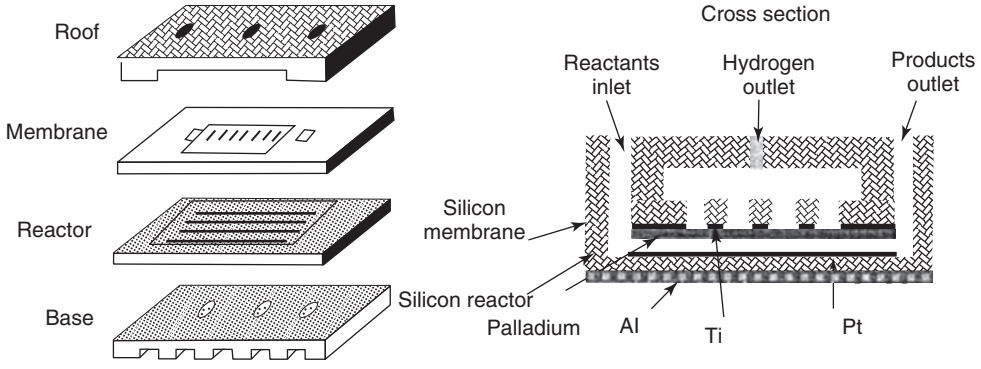

Figure 6.14 Membrane microreactor designed. (Adapted from Ref. [67].)

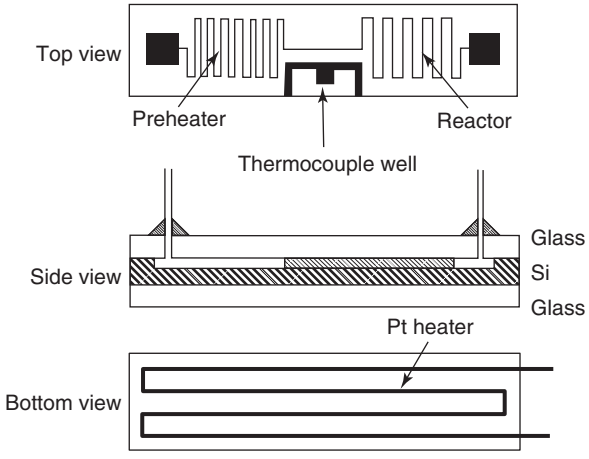

Figure 6.15 A silicon-based microchip MSR with Pt heater. (Reproduced from Ref. [68] With kind permission of Springer Science+Business Media.)

Two silicon reactors with different channel systems manufactured by photolithography and KOH etching were used for cyclohexene (de)hydrogenation over Pt catalysts [69]. In the first reactor, 39 channels of 100 μm width revealing a total surface area of 2 cm^2 were incorporated, the second one had 780 channels of 5 μm width manufactured by ion coupled plasma (ICP) etching with a total surface area of 28 cm^2. The Pt catalyst was introduced by sputtering. Higher conversions were obtained in smaller reactors because of the higher surface area and thus catalyst mass of the smaller channel system, which results in a higher modified residence time (catalyst mass/flow rate).

The above channel systems were modified using dip-coating, spin-coating, and drop-coating to introduce silica as a porous layer [70]. Pt was then introduced

by both sputtering and wet impregnation. The resulting surface areas increased from 1000 to 15 000 times. Selectivity toward benzene was favored at temperatures exceeding 150 °C. The lifetime of the supported catalyst was 3.5 times higher compared to their unsupported counterparts.

6.6.3 Catalytic Dehydration

A glass MSR was used to perform the dehydration of ethanol. The microchannel of size 200 × 80 µm deep × 30 mm (in a "Z" shaped configuration) was produced by photolithographic etching [71]. A sulfated zirconia catalyst immobilized over the surface of the top cover block. In addition, a NiCr wire was immobilized in the reactor cover as a heating device. At a reaction temperature of 155 °C and a flow rate of 3 µl min^{-1} the main products were 68% ethylene, 16% ethane, and 15% methane. A further increase of the residence time resulted in a reaction progress beyond dehydration to almost complete cracking of the ethanol to methane.

6.6.4 Ethylene Oxide Synthesis

The reactor used for ethylene oxide synthesis consisted of a two-piece housing that was sealed by graphite gaskets [72]. In the recesses, stacks of platelets of microchannels were inserted. The first recess contained a stack of mixer platelets made by a combination of Laser-LIGA (briefed in chapter 1) and electroforming. These platelets had curved microchannels that made the fluid turn by 90°. Two types of mirror-imaged platelet designs allowed in an alternating stack arrangement for creating gas multilamellae. The second recess with a stack of silver reaction platelets made by LIGA and electroforming and chemically etched silver and milled "aluchrom" (aluminum containing stainless steel) platelets were used. Heating the aluchrom material to 1100 °C with oxygen creates an α-Al_2O_3 surface, which is the only alumina species active for the ethylene reaction. The surface of the silver reaction channels was enhanced by a factor of 2–3 by means of oxidation. The silver catalyst was introduced by sputtering. The reactor demonstrated safe operation of a highly explosive reaction mixture (explosion of ethylene oxide in air 2.6–100 vol% at ambient pressure) [73]. Contrary to the industrial process that applies alumina, supported pure silver was used as catalyst for the reaction with external heating and operated at 300 °C and 25 bar. The space time yields achieved were 0.18–0.67 t m^3 h^{-1}, which is superior compared to the industrial process (Figure 6.16).

Further [73] silver wafers were also used for ethylene oxide synthesis [74]. Easy handling and fast exchange of catalyst platelets were fabricated by means of thin-wire µEDM (micro electrical discharge machining) in aluminum or aluminum alloys such as Dural, $AlMg_3$, and AlMg 4.5Mn. The rough surface of the microchannels regarded as beneficial for the coating techniques

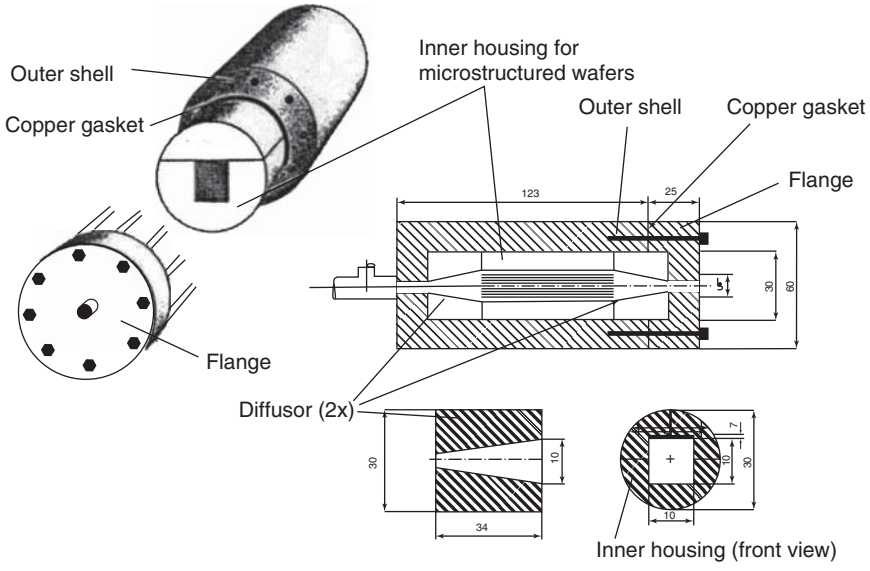

Figure 6.16 Modular microchannel reactor for gas–solid reactions. (Adapted from Ref. [74].)

applied subsequently. Both anodic oxidation and the sol–gel method were used to get a porous alumina carrier. The active compound, silver, was introduced by sputtering in both cases. A stepwise increase of the silver layer thickness from 100 to 400 nm increased conversion at constant catalyst selectivity.

6.6.5 Steam Reforming

A silicon-chip in a stainless steel housing, electrically heated and sealed with graphite, for hydrogen production from methanol steam reforming was used [75]. The microchannel was a long serpentine of 1000 µm width and 230 µm depth fabricated by photolithography and KOH etching. Cu catalyst was sputtered to a thickness of 33 nm onto the chip. Preliminary simulations revealed nonuniform temperature distribution in the reactor housing pointing at the importance of proper insulation especially in low power systems. At a feed composition of 76 mol% methanol in steam less than 7% conversion was achieved at 250 °C.

In another reactor carrying microstructured plates, a copper-based low temperature water–gas-shift catalyst was applied [76]. The reactor took up 20 plates made of FeCrAl alloy with channel size 200 × 100 µm. The kinetic measurements were carried out and expressions were determined for both a tubular fixed bed reactor containing 30 mg catalyst particles and the microreactor coated with the

catalyst particles. The reaction rate was on an average 34% higher for the coated catalysts.

6.6.6
Fischer–Tropsch Synthesis

A silicon-chip-based reactor was applied for the Fischer–Tropsch synthesis using an iron catalyst [77]. The chips had outer dimensions of 1×3 cm with channel dimensions of 5 or 100 μm width at 50–100 μm depth. The reaction was carried out at a H_2/CO ratio of 3, and flow rates of 0.4 std. $cm^3\ min^{-1}$ between 200 and 250 °C. Conversions between 50 and 70% were found after 12 h activation of the catalyst under reaction conditions.

6.7
Summary

In this chapter, the various characteristics of MSR for fluid–solid reactions are presented. It is clear that microreactors are mostly suitable for reactions that have fast intrinsic kinetics and require rapid transport, are carried out at high temperatures and pressures, and, therefore, ensure inherent safety. Effective exploitation of the full chemical potential of catalysts through high rates of heat and mass transfer provides an excellent means for identifying novel synthesis routes that are both economically attractive and environmentally benign.

The time available for chemical transformation in the MSR is very short because of their small size, which results in low hold-ups, on one hand, but necessitates highly efficient mass/heat transfer, on the other. The amount of power dissipation for multiphase reactions per unit of interfacial area is very low, leading to significant reductions in the energy consumption.

Several examples reported show precise control of the operating conditions resulting in increased selectivity toward the target compound. Higher conversion rates were achieved by processing at high pressure and high temperature, often in the explosive regime, increasing space time yield as compared to conventional reactors. Many examples of partial oxidations were described with the processes of utmost industrial importance. Within consecutive processes, high selectivity was achieved for species that are thermodynamically not the most stable molecule of all species serially generated [57]. In many cases, the better reactor performance as compared to fixed bed technology was achieved.

Nevertheless, there are several constraints hampering the use of microstructured devices for fluid–solid reactions. In the catalytic reactions, the performance is very adversely affected by catalyst deactivation. Effective *in situ* catalyst regeneration thus becomes necessary, as the simple catalyst change practiced in conventional reactors is usually no longer an option. The thickness of the catalytic wall is often greater than the internal diameter of the channel and, therefore, may impede heat transfer for highly exothermic reactions leading to nonisothermal behavior.

Reactions involving highly viscous materials or suspended particles are difficult to carry out in the microreactor.

6.8 List of Symbols

A_p, A_{foam}	Outer surface area of pallet, outer surface area of foam	m^2
a, a_{bed}, a_{struc}, a_{foam}, a_p, a_R, a_v $a_{v,\text{foam}}$	Catalytic surface area per reactor volume, of randomly packed bed, of microchannels, specific surface area per foam volume, specific surface area of the pellet, specific surface area referred to reaction volume, specific surface area referred to void volume, specific surface area of foam referred to void volume	$m^2\ m^{-3}$
$A_{\text{CS, bed}}$, $A_{\text{CS, struc}}$	Cross-section area of packed bed, of structured bed	m^2
DaI_m	First Damköhler number based on mass transfer rate	—
d_c, d_p, d_w	Cell diameter, diameter of pallet or pore, diameter of wire (catalytic filament)	m
d_s	Mean strut thickness	m
L_{bed}, L_{struc}, L_e	Length of randomly packed bed, length of structured bed, length of the entrance zone	m
L_{circ}	Perimeter	m
Re_p, Re_f	Particle Reynolds number, foam Reynolds number,	—
Sh_p, Sh_f	particle Sherwood number, foam Sherwood number,	—
Sh'_∞, Sh''_∞	asymptotic Sherwood number at constant mass flow (with reaction) from the bulk to the wall, at mass transfer with chemical reaction	—
$V_{v,\text{foam}}$	Void volume of foam	m^3
u_v	Velocity in the void volume or interstitial velocity	$m\ s^{-1}$
δ_{cat}	Thickness of catalytic layer	m
ε_{bed}, $\varepsilon_{\text{foam}}$, $\varepsilon_{\text{struc}}$	Porosity of randomly packed bed, porosity of foam, porosity of structured bed or multichannel reactors	—
η_p	Internal effectiveness factor in isothermal catalyst layer	—
η_m	Mass transfer effectiveness	—

References

1. Henkel, K.-D. (2012) Reactor types and their industrial applications, in *Ullmann's Encyclopedia of Industrial Chemistry*, Wiley-VCH Verlag GmbH, Weinheim.
2. Cybulski, A. and Moulijn, J.A. (eds) (2006) *Structured Catalysts and Reactors*, 2nd edn, Taylor & Francis Group, Boca Raton, FL, London, New York.

3. Jensen, K.F. (2001) Microreaction engineering – is small better? *Chem. Eng. Sci.*, **56** (2), 293–303.
4. Rodemerck, U., Ignaszewski, P., Lucas, M., Claus, P., and Baerns, M. (2000) *Proceedings of the 3rd International Conference on Microreaction Technology, IMRET 3*, Springer, Frankfurt am Main, pp. 287–293.
5. Ajmera, S.K., Delattre, C., Schmidt, M.A., and Jensen, K.F. (2001) *Proceedings of the 5th International Conference on Microreaction Engineering (IMRET 5)* (ed. W. Ehrfeld), Springer: Strasbourg. pp. 414-423.
6. Bakhtiary-Davijany, H., Hayer, F., Phan, X.K., Myrstad, R., Venvik, H.J., Pfeifer, P., and Holmen, A. (2011) Characteristics of an integrated micro packed bed reactor-heat exchanger for methanol synthesis from syngas. *Chem. Eng. J.*, **167** (2-3), 496–503.
7. Hayer, F., Bakhtiary-Davijany, H., Myrstad, R., Holmen, A., Pfeifer, P., and Venvik, H.J. (2013) Characteristics of integrated micro packed bed reactor-heat exchanger configurations in the direct synthesis of dimethyl ether. *Chem. Eng. Process.*, **70**, 77–85.
8. Wolfrath, O., Kiwi-Minsker, L., Reuse, P., and Renken, A. (2001) Novel membrane reactor with filamentous catalytic bed for propane dehydrogenation. *Ind. Eng. Chem. Res.*, **40**, 5234–5239.
9. Horny, C., Kiwi-Minsker, L., and Renken, A. (2004) Micro-structured string-reactor for autothermal production of hydrogen. *Chem. Eng. J.*, **101** (1-3), 3–9.
10. Horny, C., Renken, A., and Kiwi-Minsker, L. (2007) Compact string reactor for autothermal hydrogen production. *Catal. Today*, **120** (1), 45–53.
11. Kiwi-Minsker, L. (2002) Novel structured materials for structured catalytic reactors. *Chimia*, **56** (4), 143–147.
12. Patcas, F.C., Garrido, G.I., and Kraushaar-Czarnetzki, B. (2007) CO oxidation over structured carriers: a comparison of ceramic foams, honeycombs and beads. *Chem. Eng. Sci.*, **62** (15), 3984–3990.
13. Tadd, A.R., Gould, B.D., and Schwank, J.W. (2005) Packed bed versus microreactor performance in autothermal reforming of isooctane. *Catal. Today*, **110** (1-2), 68–75.
14. Buciuman, F.C. and Kraushaar-Czarnetzki, B. (2003) Ceramic foam monoliths as catalyst carriers. 1. Adjustment and description of the morphology. *Ind. Eng. Chem. Res.*, **42** (9), 1863–1869.
15. Yu, H., Chen, H., Pan, M., Tang, Y., Zeng, K., Peng, F., and Wang, H. (2007) Effect of the metal foam materials on the performance of methanol steam microreformer for fuel cells. *Appl. Catal. Gen.*, **327** (1), 106–113.
16. Moritz, T., Lenk, R., Adler, J., and Zins, M. (2005) Modular micro reaction system including ceramic components. *Int. J. Appl. Ceram. Technol.*, **2** (6), 521–528.
17. Kiwi-Minsker, L., Yuranov, I., Siebenhaar, B., and Renken, A. (1999) Glass fiber catalysts for total oxidation of CO and hydrocarbons in waste gases. *Catal. Today*, **54**, 39–46.
18. Yuranov, I., Kiwi-Minsker, L., and Renken, A. (2003) Structured combustion catalysts based on sintered metal fibre filters. *Appl. Catal. Environ.*, **43**, 217–227.
19. Yuranov, I., Renken, A., and Kiwi-Minsker, L. (2005) Zeolite/sintered metal fibers composites as effective multi-structured catalysts. *Appl. Catal.*, **281** (1-2), 55–60.
20. Nikolajsen, K., Kiwi-Minsker, L., and Renken, A. (2006) Structured fixed-bed adsorber based on zeolite/sintered metal fibre for low concentration VOC removal. *Chem. Eng. Res. Des.*, **84** (A7), 562–568.
21. Luther, A., Brandner, J.J., Schubert, K., Renken, A., and Kiwi-Minsker, L. (2008) Novel design of a microstructured reactor allowing fast temperature oscillations. *Chem. Eng. J.*, **135**, S254–S258.
22. Bromley, B., Hessel, V., Renken, A., and Kiwi-Minsker, L. (2008) "Sandwich reactor" for heterogeneous catalytic processes: N2O decomposition as a case study. *Chem. Eng. Technol.*, **31** (8), 1162–1169.

23. Haas-Santo, K., Gorke, O., Pfeifer, P., and Schubert, K. (2002) Catalyst coatings for microstructure reactors. *Chimia*, **56** (11), 605–610.
24. Renken, A. and Kiwi-Minsker, L. (2010) Microstructured catalytic reactors. *Adv. Catal.*, **53**, 47–122.
25. Hönicke, D. and Wiessmeier, G. (1996) Microsystem technology for chemical and biological microreactors. *DECHEMA Monogr.*, **132**, 93–107.
26. Wiessmeier, G. and Honicke, D. (1996) Microfabricated components for heterogeneously catalysed reactions. *J. Micromech. Microeng.*, **6** (2), 285–289.
27. Wiessmeier, D., K. Schubert, and D. Hönicke (1997) *IMRET1, 1st International Conference on Microreaction Technology*, Springer, Berlin, 1997, pp. 20–26.
28. Ganley, J.C., Riechmann, K.L., Seebauer, E.G., and Masel, R.I. (2004) Porous anodic alumina optimized as a catalyst support for microreactors. *J. Catal.*, **227** (1), 26–32.
29. Brinker, C.J. and Scherer, G.W. (1990) *Sol-Gel Science*, Academic Press.
30. Gonzalez, R.D., Lopez, T., and Gomez, R. (1997) Sol-gel preparation of supported metal catalysts. *Catal. Today*, **35** (3), 293–317.
31. Reuse, P. (2003) Production d'hydrogéne dans un réacteur microstructuré. Couplage themque entre le steam reforming et l'oxydation totale du méthanol. PhD Thesis. EPFL, Lausanne.
32. Rouge, A. and Renken, A. (2001) Performance enhancement of a microchannel reactor under periodic operation. *Stud. Surf. Sci. Catal.*, **133**, 239–246.
33. Pfeifer, P., Bohn, L., Görke, O., Haas-Santo, K., Schygulla, U., and Schubert, K. (2005) Microstructured mixers for gas-phase processes – manufacture, characterization and applications. *Chem. Eng. Technol.*, **28** (4), 439–445.
34. Coronas, J. and Santamaria, J. (2004) The use of zeolite films in small-scale and micro-scale applications. *Chem. Eng. Sci.*, **59** (22-23), 4879–4885.
35. Hiemer, U., Klemm, E., Scheffler, F., Selvam, T., W.S. , and Emig, G. (2004) Microcreation engineering studies of the hydroxylation of benzene with nitrous oxide. *Chem. Eng. J.*, **101** (1-3), 17–22.
36. Rebrov, E.V., Seijger, G.B.F., Calis, H.P.A., de Croon, M., van den Bleek, C.M., and Schouten, J.C. (2001) The preparation of highly ordered single layer ZSM-5 coating on prefabricated stainless steel microchannels. *Appl. Catal., A*, **206** (1), 125–143.
37. Louis, B., Kiwi-Minsker, L., Reuse, P., and Renken, A. (2001) ZSM-5 coatings on stainless steel grids in one-step benzene hydroxylation to phenol by N_2O: Reaction kinetics study. *Ind. Eng. Chem. Res.*, **40** (6), 1454–1459.
38. Louis, B., Reuse, P., Kiwi-Minsker, L., and Renken, A. (2001) Synthesis of ZSM-5 coatings on stainless steel grids and their catalytic performance for partial oxidation of benzene by N2O. *Appl. Catal. Gen.*, **210** (1-2), 103–109.
39. Janicke, M.T., Kestenbaum, H., Hagendorf, U., Schuth, F., Fichtner, M., and Schubert, K. (2000) The controlled oxidation of hydrogen from an explosive mixture of gases using a microstructured reactor/heat exchanger and Pt/Al_2O_3 catalyst. *J. Catal.*, **191** (2), 282–293.
40. Thybo, S., Jensen, S., Johansen, J., Johannessen, T., Hansen, O., and Quaade, U.J. (2004) Flame spray deposition of porous catalysts on surfaces and in microsystems. *J. Catal.*, **223** (2), 271–277.
41. Schimpf, S., Bron, A., and Claus, P. (2004) Carbon-coated microstructured reactors for heterogeneously catalyzed gas phase reactions: influence of coating procedure on catalytic activity and selectivity. *Chem. Eng. J.*, **101** (1-3), 11–16.
42. Tribolet, P. and Kiwi-Minsker, L. (2005) Carbon nanofibers grown on metallic filters as novel catalytic materials. *Catal. Today*, **102**, 15–22.
43. Commenge, J.-M., Falk, L., Corriou, J.-P., and Matlosz, M. (2002) Optimal design for flow uniformity in microchannel reactors. *AIChE J.*, **48** (2), 345–358.
44. Wirth, K.-E. (2010) Pressure drop in fixed beds, Part L1.6, in *VDI-Heat Atlas*, Springer, Berlin, New York, Heidelberg.
45. Dietrich, B., W.S. , Kind, M., and Martin, H. (2009) Pressure

drop measurements of ceramic sponges—determining the hydraulic diameter. *Chem. Eng. Sci.*, **64** (16), 3633–3640.
46. Dietrich, B. (2012) Pressure drop correlation for ceramic and metal sponges. *Chem. Eng. Sci.*, **74**, 192–199.
47. Perry, R.H., Green, D.W., and Maloney, J.O. (1997) *Perry's Chemical Engineers' Handbook*, 7th edn, McGraw-Hill.
48. Incera Garrido, G., Patcas, F.C., Lang, S., and Kraushaar-Czarnetzki, B. (2008) Mass transfer and pressure drop in ceramic foams: a description for different pore sizes and porosities. *Chem. Eng. Sci.*, **63** (21), 5202–5217.
49. Incera Garrido, G. and Kraushaar-Czarnetzki, B. (2010) A general correlation for mass transfer in isotropic and anisotropic solid foams. *Chem. Eng. Sci.*, **65** (6), 2255–2257.
50. Mears, D.E. (1971) Tests for transport limitations in experimental catalytic reactors. *Ind. Eng. Chem. Process Des. Develop.*, **10** (4), 541–547.
51. Sherony, D.F. and Solbrig, C.W. (1970) Analytical investigation of heat or mass transfer and friction factors in a corrugated duct heat or mass exchanger. *Int. J. Heat Mass Transfer*, **13** (1), 145–146.
52. Hoebink, J.H.B.J. and G.B. Marin, Modeling of monolithic reactors for automotive exhaust gas treatment, in *Structured Catalysts and Reactors*, J.A.M. A. Cybulski, Ed 1998, Marcel Dekker, Inc.: New York.
53. Cybulski, A. and Moulijn, J.A. (1994) Monoliths in heterogeneous catalysis. *Catal. Rev. Sci. Eng.*, **36** (2), 179–270.
54. Hayes, R.E. and Kolaczkowski, S.T. (1994) Mass and heat transfer effects in catalytic monolith reactors. *Chem. Eng. Sci.*, **49** (21), 3587–3599.
55. Villermaux, J. (1971) Diffusion dans un reacteur cylindrique. *Int. J. Heat Mass Transfer*, **14** (12), 1963–1981.
56. Giani, L., Groppi, G., and Tronconi, E. (2005) Mass-transfer characterization of metallic foams as supports for structured catalysts. *Ind. Eng. Chem. Res.*, **44** (14), 4993–5002.
57. Kolb, G. and Hessel, V. (2004) Microstructured reactors for gas phase reactions. *Chem. Eng. J.*, **98** (1-2), 1–38.
58. Kolb, G. (2013) Review: microstructured reactors for distributed and renewable production of fuels and electrical energy. *Chem. Eng. Process.*, **65**, 1–44.
59. Srinivasan, R., Hsing, I.M., Berger, P.E., Jensen, K.F., Firebaugh, S.L., Schmidt, M.A., Harold, M.P., Lerou, J.J., and Ryley, J.F. (1997) Micromachined reactors for catalytic partial oxidation reactions. *AIChE J.*, **43** (11), 3059–3069.
60. Jensen, K.F., Firebaugh, S.L., Franz, A.J., Quiram, D., Srinivasan, R., and Schmidt, M.A. (1998) in *Micro Total Analysis Systems* (eds J. Harrison and A. van den Berg), Kluwer Academic Publishers, Dordrecht, p. 463.
61. Franz, A.J., Jensen, K.J., and Schmidt, M.A. (1999) *Proceedings of the 3rd International Conference on Microreaction Technology*, Springer, Berlin, p. 267.
62. Schouten, J.C., Rebrov, E.V., and De Croon, M.H.J.M. (2002) Miniaturization of heterogeneous catalytic reactors: prospects for new developments in catalysis and process engineering. *Chimia*, **56** (11), 627–635.
63. Veser, G., Friedrich, G., Freygang, M., and Zengerle, R. (2000) *Proceedings of the 3rd International Conference on Microreaction Technology 1999*, Springer, Berlin, p. 674.
64. Veser, G. (2001) Experimental and theoretical investigation of H2 oxidation in a high-temperature catalytic microreactor. *Chem. Eng. Sci.*, **56** (4), 1265–1273.
65. Cao, E., Yeong, K.K., Gavriliidis, A., Cui, Z., and Jenkins, D.W.K. (2002) *Proceedings of the 6th International Conference on Microreaction Technology*, AIChE, New York, pp. 76–84.
66. Alepee, C., Maurer, R., Paratte, L., Vulpescu, L., Renaud, P., and Renken, A. (2000) Fast heating and cooling for high temperature chemical microreactors. *Microreact. Technol.: Ind. Prospects*, 514–525.
67. Zheng, A., Jones, F., Fang, J., and Cui, T. (2000) *Proceedings of the 4th International Conference on Microreaction Technology*, AIChE, New York, pp. 284–292.
68. Kusakabe, K., Miyagawa, D., Gu, Y., Maeda, H., and S.M. (2001) *Proceedings 5th International Conference on*

Microreaction Technology, Springer, Berlin, pp. 70–77.

69. Surangalikar, H., Ouyang, X., and Besser, R.S. (2003) Experimental study of hydrocarbon hydrogenation and dehydrogenation reactions in silicon microfabricated reactors of two different geometries. *Chem. Eng. J.*, **93** (3), 217–224.
70. Zhao, S. and Besser, R.S. (2002) *Proceedings of the 6th International Conference on Microreaction Technology*, AIChE, New York, pp. 289–296.
71. Wilson, N.G. and McCreedy, T. (2000) On-chip catalysis using a lithographically fabricated glass microreactor - the dehydration of alcohols using sulfated zirconia. *Chem. Commun.*, **9**, 733–734.
72. Löwe, H., W.E. , Gebauer, K., Golbig, K., Hausner, O., Haverkamp, V., Hessel, V., and Richter, T. (1998) *Proceedings of the 2nd International Conference on Microreaction Technology*, AIChE, New York, pp. 63–74.
73. Kestenbaum, H., De Oliveira, A.L., Schmidt, W., Schüth, F., Ehrfeld, W., Gebauer, K., Löwe, H., Richter, T., Lebiedz, D., Untiedt, I., and Zücher, H. (2002) Silver-catalyzed oxidation of ethylene to ethylene oxide in a microreaction system. *Ind. Eng. Chem. Res.*, **41** (4), 710–719.
74. Kursawe, A., Pilz, R., Dürr, H., and Hönicke, D. (2000) *Proceedings of the 4th International Conference on Microreaction Technology*, AIChE, New York, pp. 227–235.
75. Pattekar, A.V., Kothare, M.V., Karnik, S.V., and Hatilis, M.K. (2001) *Proceedings of the 5th International Conference on Microreaction Technology*, Springer, Berlin, pp. 332–342.
76. Reuse, P., P. Tribolet, L. Kiwi-Minsker, and A. Renken (2001) *Proceedings of the 5th International Conference on Microreaction Technology*. Springer, Berlin. pp. 322-331
77. Besser, R., Ouyang, X., and Surangalikar, H. (2002) *Proceedings of the 6th International Conference on Microreaction Technology*, AIChE, New York, pp. 254–261.